Zhang Jie (Orcid ID: 0000-0002-9204-9834)

Impact of the eastward shift in the negative-phase NAO on extreme drought over northern China in summer

Yibo Du[1], Jie Zhang[1*], Siwen Zhao[1]

1 Key Laboratory of Meteorological Disaster, Ministry of Education (KLME)/Joint International Research Laboratory of Climate and Environment Change (ILCEC)/Collaborative Innovation Center on Forecast and Evaluation of Meteorological Disasters (CIC-FEMD), Nanjing University of Information Science & Technology, Nanjing 210044, China

Corresponding author: Jie Zhang, Zhangj@nuist.edu.cn

Abstract: The frequency of extreme drought events in northern China has increased since the mid-1990s, and such a decadal anomalous trend may have a vital influence on national economics and food supply. Based on the analysis of observational datasets and experiments conducted by a linear baroclinic model, this study claims that the intraseasonal circulation anomalies related to extreme drought are linked to the eastward shift in the negative phase of the summer North Atlantic Oscillation (SNAO).

This article has been accepted for publication and undergone full peer review but has not been through the copyediting, typesetting, pagination and proofreading process which may lead to differences between this version and the Version of Record. Please cite this article as doi: 10.1029/2019JD032019

When the SNAO is in a negative phase, the cyclonic eddy-driven jet can enhance the eastward extension of the North Atlantic jet stream (NAJS), contributing to a closer connection between the NAJS and the Asian-African jet stream and enhancing the waveguide. The cyclonic eddy in the exit of the jet stream excites anomalous Rossby wave energy that originates from the NAJS exit and spreads to the Caspian Sea, Mongolia, and northern China; this associated wave train, which is similar to the Silk Road Pattern (SRP), enhances the anticyclonic anomaly over northern China, establishing a pronounced link with extreme drought in northern China. Thus, the negative phase of the SNAO may be a contributing driver of extreme drought in northern China.

Key words: SNAO, extreme droughts, North Atlantic jet stream

Introduction

1. Introduction

Northern China has suffered from severe droughts since the mid-1990s; these droughts can seriously stress the balance among the economy, society, and environment. Historical records have shown that northern China has suffered from consecutive years of drought since the 1980s. For example, the Yellow River and Huaihe River dried up in 1997 and 1999, respectively (Ma and Fu, 2006; Zhang et al., 2009). During the 2000s, drought events occurred in northern China in 4 consecutive years (Zhang et al., 2015). Under the background of significant global warming, the intensity and frequency of droughts have both increased, especially in 2005 and 2010 in northern Shanxi Province and Henan Province. These events illustrate that there is an increasing tendency in the occurrence and duration of droughts.

Previous studies have shown that anomalies of both westerly and summer monsoon circulations can lead to extreme drought in northern China (Huang et al., 2007; Wu et al., 2009). In terms of summer

monsoon-related circulations, weakened Asian monsoon circulation can increase the frequency of drought in northern China due to inadequate water vapor transport (Zhang and Zhou, 2015). In addition, the predominant teleconnection, referred to as the Pacific-Japan (PJ) pattern (Nitta, 1987), exhibits an anticyclonic anomaly over northern China in drought years. Considering the westerly anomaly, drought in northern China corresponds to an enhancement in meridional circulation and low-frequency waves, such as the Silk Road Pattern (SRP, Zhang et al.,2019), a teleconnection pattern spanning across the Eurasian continent along the Asian westerly jet (Lu et al., 2002; Hong and Lu. 2016). The latter could strengthen meridional circulation under the propagation of stationary wave, which is then linked with upstream turbulence and remote forcing. Some studies have shown that tropical heating can play a role in triggering the SRP (Chen and Huang. 2012).

Upstream of the low-frequency wave, the North Atlantic Oscillation (NAO, Walker, 1924), characterized by the Azores high and the Icelandic low that enhance (weaken) in the positive (negative) phase of the NAO, is the dominant mode of atmospheric variability over the North Atlantic (Wallace and Gutzler, 1981; Hurrell, 1995). Many previous studies have shown that the NAO phase shift can result in a wide range of weather and climate anomalies in the Northern Hemisphere (Hurrell, 1995; Huang et al., 1998; Hurrel et al., 2003; Li et al., 2013). The phase shift from the positive to negative NAO changes the North Atlantic storm track intensity, frequency and path, which can cause abnormal transport and convergence of water vapor (Rogers, 1997; Hurrel and van Loon, 1997), leading to a wet (dry) and rainy (sunny) climate in northern (southern) Europe. In addition to the influence of the NAO on Europe, the NAO pattern also impacts the weather and climate in Asia, and the positive phase of the NAO is favorable for a weaker Siberian high and shallower East Asian trough, which can further result in the weakening of the East Asian winter monsoon (Wu and Wang, 2002; Qiao and Feng, 2016).Likewise, the summer NAO (SNAO) is an important circulation anomaly at middle and high latitudes (Folland et al., 2009). Previous studies have shown that the SNAO has a vital influence on the climate, including the influence on summer

air temperature and rainfall in the Northern Hemisphere (Yuan and Sun, 2009; Hurrell and Folland, 2002; Linderholm et al., 2011). Some studies have suggested that extremely wet conditions in Northern Europe and extremely dry conditions in the Mediterranean region are related to the location of the North Atlantic jet stream when the SNAO is in the negative phase (Blackburn et al., 2008; Richard Hall et al., 2014). Except for the simultaneous influence of the NAO, Wu et al. (2009) found that the positive (negative) phase of the NAO could force a tripole mode "+, -, +" ("-, +, -") anomaly in the North Atlantic sea surface temperature (SST) in spring and that this tripole mode SST anomaly could persist into summer and excite the wave train teleconnection over northern Eurasia (Gu et al., 2009; Wu et al., 2009; Zuo et al., 2013).

However, the relationships between the SNAO and climate anomalies over northern China are not clear. Wang (2018) suggested that the SNAO has led to precipitation anomalies over northern China by altering the thermal forcing of the Tibetan Plateau. In fact, the SNAO is a forcing source that can cause circulation and wave anomalies and has experienced a decadal change after the 1970s, with the southern center shifting eastward (Sun et al., 2008a; Sun et al., 2009b; Sun and Wang, 2012). Thus, the connection between the decadal change in the SNAO pattern and the frequent occurrence of extreme events over East Asia may be strengthened. However, there is a lack of evidence that extreme droughts over northern China respond to the impact of the SNAO. Motivated by this uncertainty, the impact of the SNAO on extreme drought over northern China in summer and its possible mechanisms are analyzed in this paper.

This article is organized as follows. Section 2 introduces the data and methods used. In section 3, the relationship between the SNAO and extreme drought over northern China and its possible physical mechanism are investigated. Finally, the conclusions are presented in section 4.

2. Data and Methods

2.1 Datasets

The ERA-Interim reanalysis data (http://apps.ecmwf.int/datasets/) from the European Centre for Medium-Range Weather Forecasting, including the monthly mean values of the zonal and meridional winds, geopotential height, and air temperature, are adopted. This dataset has 1°×1° horizontal resolution and 16 vertical levels that extend from 1000 hPa to 50 hPa. The observation precipitation dataset, with a resolution of 2.5°×2.5°, is from the Global Precipitation Climatology Project (GPCP). The monthly mean NAO indices are acquired from the Climate Prediction Center (CPC) website (ftp://ftp.cpc.ncep.noaa.gov/cwlinks). The data used in the paper are mainly for the period from 1979 to 2017. We estimate and remove the least squares linear trend of the time dimension from all grid points before conducting the correlation and regression, which the basic summaries can be found in Wei (2007).

Two drought indices are used here: a self-calibrating Palmer Drought Severity Index (sc-PDSI: Dai, 2011b) and the standardized precipitation index (SPI; Edwards and McKee.1997). The sc-PDSI index is more scientific and objective than the original PDSI since the sc-PDSI calibrates the PDSI by using local coefficients (Dai, 2011b). The sc-PDSI data used in this paper are obtained from the Climate Data Guide website (https://climatedataguide.ucar.edu/climate-data/palmer-drought-severity-index-pdsi) and have 2.5°×2.5° horizontal resolution. The SPI is simple to calculate and is not limited by season or terrain, and it has been widely used in previous studies (Panagiotis Angelidis, 2012).We calculated the SPI by fitting a gamma distribution to monthly mean GPCP precipitation value. The method apply a 2-parameter gamma distribution fit where the shape and scale parameters are maximum likelihood estimate as described in Thom (1958). An advantage of SPI is it can be created for differing period

of 1-to-36 months. In order to concentrate on intraseasonal character of SPI, we selected 3-month SPI (SPI-3) because the SPI-3 provides a comparison of the precipitation over a specific 3-month period with the precipitation totals from the same 3-month period for all the years included in the historical record. A relatively normal 3-month period could occur in the middle of a longer-term drought that would only be visible at longer time scales. Similarly, the resolution is same as sc-PDSI. Detailed information about the major drought indices are shown in Table 1.

2.2 Methods

Singular value decomposition (SVD) was employed to investigate the collocation patterns of correlation between the zonal wind and kinetic energy (Tk_{01}) in the jet exit, and empirical orthogonal function (EOF) analysis was employed to extract the zonal wind leading modes in the jet exit. Both of these methods have been widely used in climate diagnosis (Wang et al. 2017; Xu et al. 2019). To investigate stationary propagation, the method for calculating the wave activity flux defined by Takaya and Nakamura (1997, 2001) is used in this study. Other methods, including regression and correlation, are used to analyze the link between the physical variables and the NAO index. Statistical significance tests were assessed through Student's two-tailed t testing.

In our research, a localized multiscale energy and vorticity analysis (MS-EVA) (Liang, 2016; Liang and Robinson, 2005; Liang and Anderson, 2007) based on a new functional analysis tool called the multiscale window transform (MWT) is used to study the conversion of kinetic energy in the jet exit. The MWT is understood as a space or time orthogonal decomposition according to different scale ranges, where the local characteristics of a physical process can be preserved in the decomposition. The following is the equation for kinetic energy derived from the MS-EVA theory, and the detailed derivation process can be found in Liang（2016):

$$\frac{\partial K^{\varpi}}{\partial t} = -\nabla \cdot Q_K^{\varpi} - \nabla \cdot Q_P^{\varpi} - b^{\varpi} + \Gamma_K^{\varpi} + F_K^{\varpi} \quad (1)$$

Equation (1) can be represented as follows:

$$Kt = QK+QP+BUOY+T+R,\ T=T01+T21+T11+T201$$

K_t ($\frac{\partial K}{\partial t}$) is the rate of change in kinetic energy over time, BUOY($-b$) is the buoyancy conversion, QP($-\nabla \cdot Q_p$) is the geopotential flux, QK($-\nabla \cdot Q_k$) is the flux of kinetic energy, and R(D) is the dissipation friction of kinetic energy. T is the conversion of kinetic energy between different scales, and it has been widely used previously (Lau, 1992; Hsu, 2009). T(Γ) is the transfer of energy at different scales. T_{01} is the trans-scale transmission of kinetic energy from a large scale to seasonal average scale. T_{21} is the trans-scale transmission of kinetic energy in high-frequency components. The two components T_{11} and T_{201} are not considered because T_{11} does not contain energy for cross-scale transmission, and the magnitude of T_{201} is very small.

2.3 Model

The numerical experiments performed in this study were based on the linear baroclinic model (LBM, Watanabe and Kimoto, 2000). The LBM is a time-dependent model, and it has a horizontal resolution of T42 (triangular truncation of 42 waves) and 20 sigma (σ) levels in the vertical direction. The background state used in the experiments is the August mean climatology during 1979-2017 from the ERA-interim data. The boundary and initial conditions were determined by the model. We designed numerical experiments using an LBM forced by cyclonic anomalies at 500 hPa in the jet exit. Since the time integration of the model response approaches a steady state after 20 days when the dissipation terms are adopted, we selected the results of the 25th day from a 30-day integration as the steady results. More details associated with the model can be found in Watanabe (2004).

Table 1 Major meteorological drought indices

Index name	calculation	Advantage	Extreme drought classification	Applied

Precipitation anomaly Percentage (Zhang et al.1998)	precipition anomaly precentage against climatological mean	Reflect the drought induced by a precipitation anomaly	-80 or less	It is used in the semihumid and semiarid area when the air temperature is higher than 10°C (Zhang et al.1998,2006)
Palmer drought severity Index (Palmer 1965; Dai et al.1998)	Departure of moisture balance from a normal condition based on a water balance model	It considers both water supply and demand and a provides reflection of soil moisture deficit or surplus	-4 or less	It is frequently used in drought study over China (Zhai et al.2010)
Standardized precipitation index (Edwards and McKee.1997)	Fitting and transforming a long-term precipitation record into a normal distribution with respect to the SPI	It could be calculated on different time scales to display short and long term water supply	-1.99 to -l.60	It is used in wet and dry conditions in northwestern China and the assessment of drought hazard (Zhang et al.2009; He et al.2011)
Composite drought index (Zou and Zhang.2008)	Combination of 30-day mean and 90-day mean standardize precipitation index and 30-day mean relative moisture	Standardize drought on different time scales	2.4 or less	It is used in provincial meterological monitoring (Zou and Zhang.2008)
Effective drought index (Byun and Wilhite.1999)	Defined as a lack of in comparison with the climatological average	Can determine drought onset and end dates	-2.0 or less	It is used in the study of drought occurring in the Korea Peninsula and Japan (Lee et al.2012;Oh et al.2014)

3. Results

3.1 Characteristics of drought and its relationship with SNAO

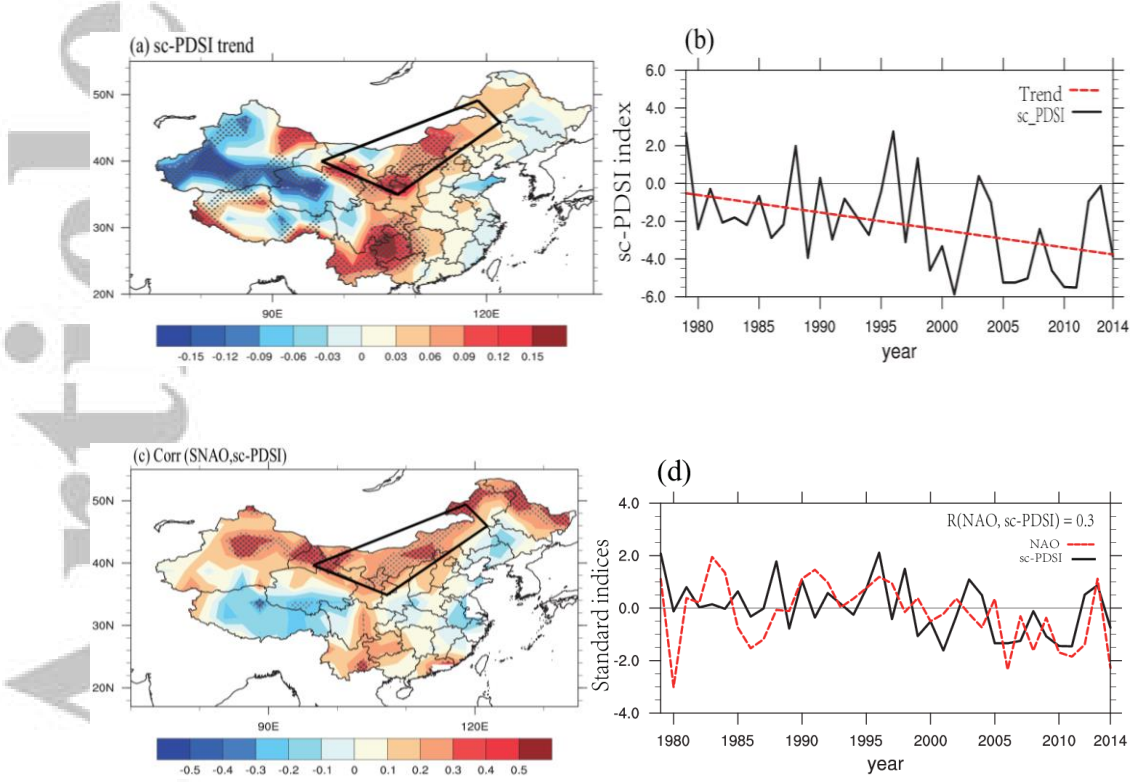

Fig. 1 (a) The trends of the sc-PDSI (×-1) in August in China from 1979 to 2014 [units:$(yr)^{-1}$]. (b) Time series of the sc-PDSI in the key region (black box area) from 1979-2014 (the sc-PDSI is currently updated through 2014). (c) Correlations between the August NAO index (SNAO) and sc-PDSI. (d) Time series of the standardized values of the SNAO and sc-PDSI in the key region from 1979-2014. The gray and black dots indicate that the trends and correlations are significant at the 90% and 95% confidence level. The black box in (a) and (c) represents the study region in this paper.

Fig. 1(a) shows that the trends are significantly positive in southwestern and northern China, while the trend in eastern China is not significant. Positive trends in southwestern and northern China indicates that drought in these regions has remarkably intensified in recent decades. Notably, the trend of sc-PDSI in northwestern China decreases, which is opposite to the trend in the key region. This contradiction may be associated with the drying trend in northern China and its shift (Ma and Fu, 2006). As shown in Fig. 1(b), the variation in the sc-PDSI in the key region substantially

decreases, implying that drought in northern China intensified during 1979-2014, and the frequency of extreme drought events (sc-PDSI ≤-4) has increased since 2000. Fig. 1(c) shows the spatial correlations distribution of SNAO and sc-PDSI. It can be seen that significant positive correlation in northern China, especially in the key region. Moreover, the standardized values of the SNAO and sc-PDSI in the key region show a positive correlation in Fig. 1(d), with a correlation coefficient of 0.3, indicating that the drought events is more likely to occur when the SNAO is in the negative phase.

3.2 Response of atmospheric circulation to the negative-phase SNAO

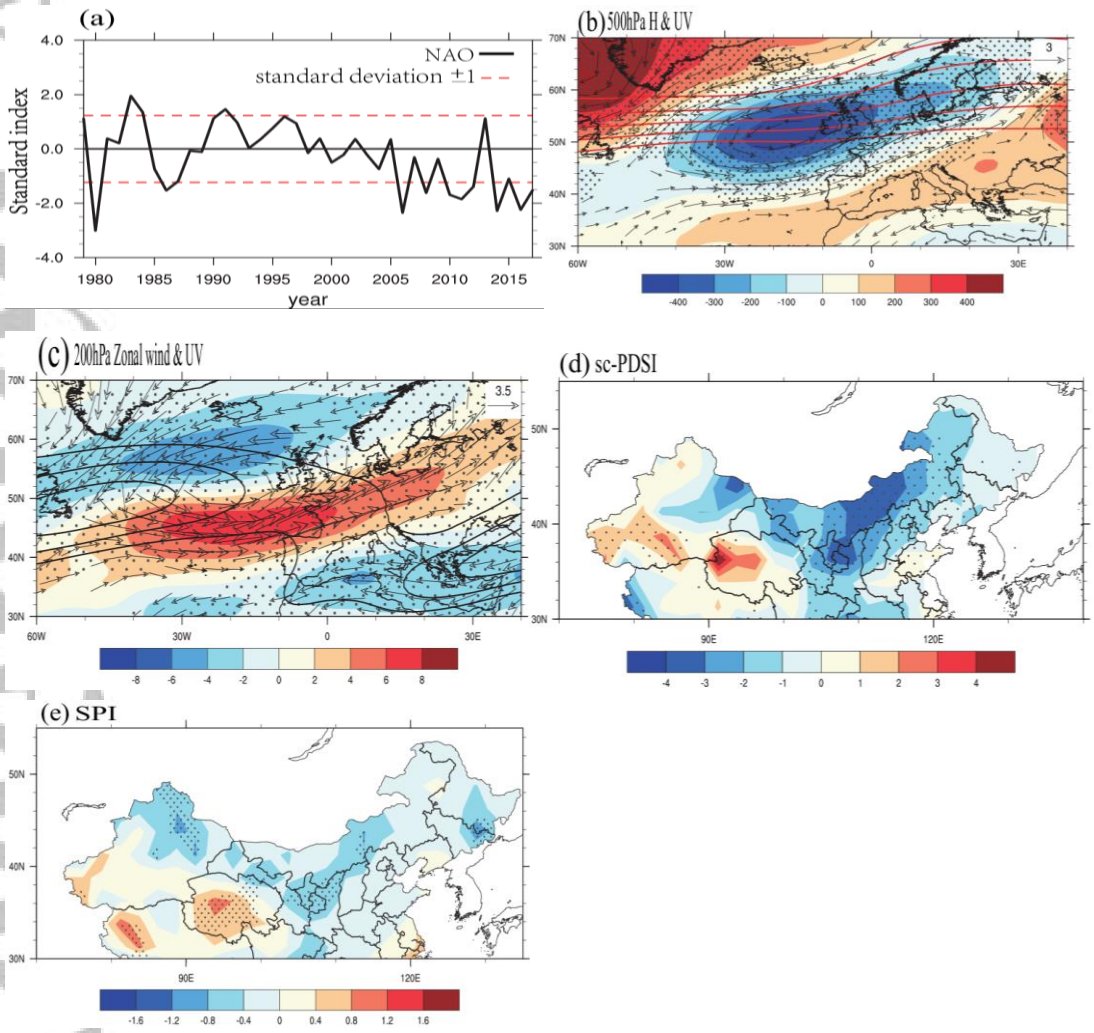

Fig. 2 (a) Time series of the standardized values of the SNAO (black line) for the period 1979-2017. (b) Composite differences of the geopotential height (gpm; shaded) and horizontal wind (m/s;

vectors) at 500 hPa between the negative-phase SNAO and the mean climate state. The red contours show the climatological isolines of the geopotential heights from 5560 to 5720 gpm. (c) Same as in (b) but for the zonal wind (m/s; shaded) and horizontal winds (m/s; vectors) at 200 hPa. The climatological zonal wind, which is greater than 15 m/s, is represented by the black contours. (e) and (d) are the same as in (b) but for the sc-PDSI and SPI, respectively. The black dots indicate that the anomalies are significant at the 95% confidence level.

The SNAO shifted to a predominantly negative phase after 2000 in Fig. 2(a). Coincidentally, extreme drought events in the key region became more frequent after the NAO phase shift (Fig. 1(b)). We defined SNAO events as negative when the SNAO index was smaller than -1.0. Therefore, the years with negative SNAO events and extreme drought events are 2006, 2008, 2010, 2011, and 2014. Thus, these five years are selected as typical negative-phase SNAO years. Figure 2(b) shows the composite differences in geopotential height and wind at 500 hPa between the negative-phase SNAO and mean climate state. It can be seen from Fig. 2(b) that the geopotential height increases at 60°W near Greenland and decreases over the western coast of Europe, and this pattern depicts a negative-phase SNAO with the southern center shifting eastward. By observing the wind field, there is anomalous cyclonic circulation in the negative geopotential height anomaly center (40°N-60°N, 30°W-10°E), with an anomalous east (west) wind existing near 60°N (40°N). In addition, the negative geopotential height anomaly and anomalous cyclonic circulation are located in the climatological trough. This configuration favors the elongation of the trough, which could enhance positive vorticity advection transport in front of the trough and result in upward motion. Compared with mid-level circulation, Fig. 2(c) shows the cyclonic eddy-driven jet enhances the eastward extension of the North Atlantic jet stream (NAJS) at 200 hPa when the SNAO is in the

negative phase, and the zonal wind exhibits a pattern of negative, positive, and negative anomalies from north to south with the cyclonic eddy at 200 hPa. The westerly (easterly) anomalies of 40°N (60°N) caused by the cyclonic eddy further strengthen (weaken) the climatological westerly wind. Figures 2(d) and 2(e) show the composite differences in the sc-PDSI and SPI between the negative-phase SNAO and mean climate state. According to drought classification of sc-PDSI, Fig. 2(d) shows that extreme drought over Ningxia, northern Shaanxi Province and east-central of Inner Mongolia (key region). To obtain further evidence for extreme drought over the key region, the SPI for a 3-month time scale (SPI-3) is used here. Compared with sc-PDSI, the drought classification of SPI is weaker, but the drought distributions are similar over the key region in Fig. 2(e). This may be related to the algorithms and applicability of the SPI (McKee et al., 1993; He et al., 2011), for instance, the SPI are based on precipitation alone and are limited because they do not deal with the evaportranspiration side of the issue (Trenbert et al, 2014).

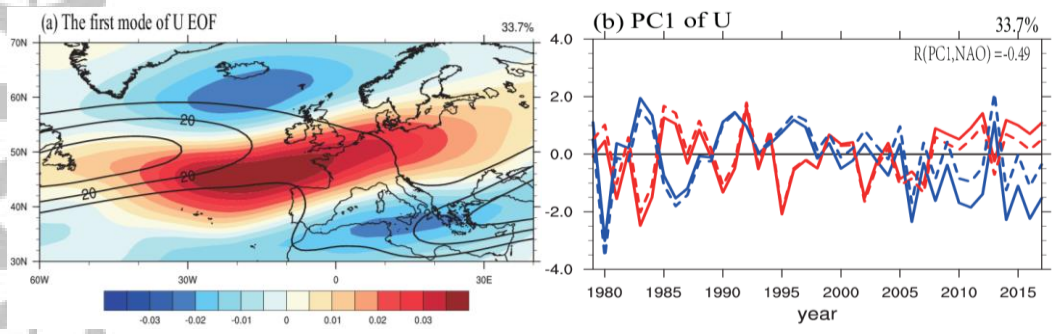

Fig. 3 (a) The leading mode of the EOF for zonal wind anomalies at 200 hPa in August and (b) the corresponding normalized leading principal component (red line). The units are arbitrary. The climatological zonal wind, which is greater than 15 m/s, is represented by the black contour line. The blue line in (b) represents the SNAO. The dashed lines correspond to the results with the linear trend removed.

Zuo et al. (2015, 2016) proved that the negative-phase NAO could affect surface temperature in

southern China by weakening the Middle East jet stream in winter, implying that the jet stream may play an important role in linking the SNAO and extreme drought anomalies over northern China. Figure 3(a) indicates the first leading mode of the EOF for the zonal wind anomalies at 200 hPa over the North Atlantic region (30°N-70°N, 60°W-40°E), and the variance in the first mode is 33.7%. The EOF mode clearly shows a negative, positive, and negative anomaly pattern from north to south, which is similar to the distribution of the zonal wind in the negative phase of the SNAO (see Fig. 2(c)), and the eastward extension of the NAJS in the exit results in conjunction of NAJS and the Asian-African jet stream and strengthening of the Asian-African jet waveguide. Moreover, the NAJS anomaly possibly increases barotropic energy transfer to kinetic energy (Zhang et al, 2019). It can be seen from Fig. 3(b) that the correlation between the PC1 and SNAO is significant at the 99% confidence level with a value of -0.49, indicating that the NAJS is more likely to extend eastward in the exit when the SNAO is in the negative phase. The relation between NAJS and SNAO emphasizes that NAJS position and speed variability are related to the SNAO edd-driven jet and Euro-Atlantic pattern (Hall et al, 2014).

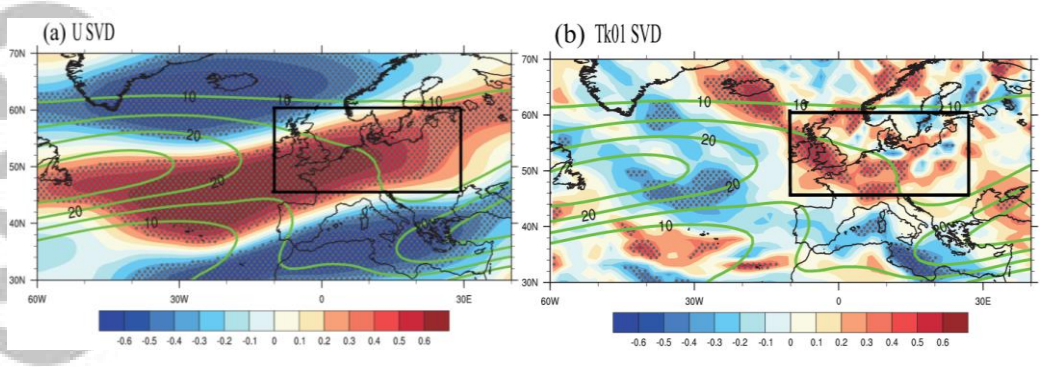

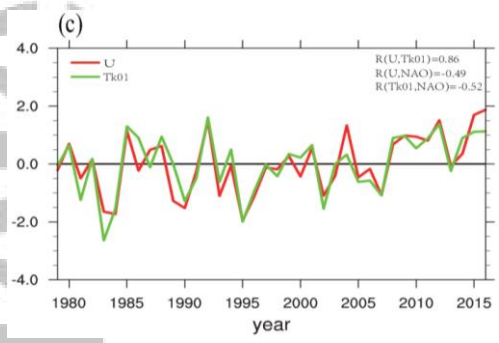

Fig. 4 Heterogeneous correlation map of the leading mode of the SVD for the (a) 200 hPa zonal wind and (b) 200 hPa Tk_{01}. (c) Normalized leading principal component of the zonal wind (red line) and Tk_{01} (green line). The units are arbitrary. The climatological zonal wind, which is larger than 10 m/s, is represented by the green contours in (a) and (b). The black dots in (a) and (b) indicate that the anomalies are significant at the 95% confidence level.

Some studies have found that the displacement of the jet stream is dominated by barotropic motion, and barotropic kinetic energy in the jet exit is easily converted (Wiin and Drake, 1965; Eastin and Vincent, 1998). Thus, the barotropic kinetic energy conversion in the jet exit may be related to the eastward extension of the NAJS. Using the localized MS-EVA methodology to obtain the kinetic energy (Tk_{01}), the positive Tk_{01} corresponds to the conversion of barotropic kinetic energy to seasonal scale kinetic energy, and the negative Tk_{01} corresponds to opposite of kinetic energy conversion (Liang XS, 2005). To investigate the relationship between the zonal wind and Tk_{01}, we perform SVD analysis between the zonal wind and Tk_{01} at 200 hPa over the Atlantic-Eurasian region. The results in Fig. 4 demonstrate that the first SVD (SVD1) mode of the zonal wind (Fig. 4(a)) is similar to the EOF mode of the zonal wind, especially the characteristic of eastward extension of the NAJS. The corresponding positive Tk_{01} is mainly in the jet exit (Fig. 4(b)). This indicates that the enhanced zonal wind is beneficial to the positive Tk_{01} in the jet exit, which can lead to the conversion from barotropic kinetic energy to eddy kinetic energy under barotropic

instability conditions. Therefore, the jet exit seems to be a source of kinetic energy conversion and provide kinetic energy for cyclonic eddy growth (Sasaki et al., 2012; Liang et al., 2016). Although the zonal wind has decreased over the southeast side of Greenland (60°N-70°N, 20°E-30°W), it corresponds with a positive Tk_{01}, which may be related to the enhancement of the polar front jet (Xu and Wang, 2019). The seasonal-scale kinetic energy convert to barotropic kinetic energy near the center of the NAJS (negative Tk_{01}), while the zonal wind strengthens, which is probably related to the North Atlantic SST anomaly (Woollings and Blackburn 2012). Figure 4(c) shows the normalized leading principal component of the zonal wind (red line) and PC1 of T_{K01} (green line); the correlation coefficient reaches 0.86, which demonstrates increasing zonal wind favors barotropic energy conversion in the exit. Meanwhile, the correlation coefficients between the two PC1s and the SNAO are -0.49 and -0.52, indicating barotropic energy conversion is associated with SNAO eddy-drive jet.

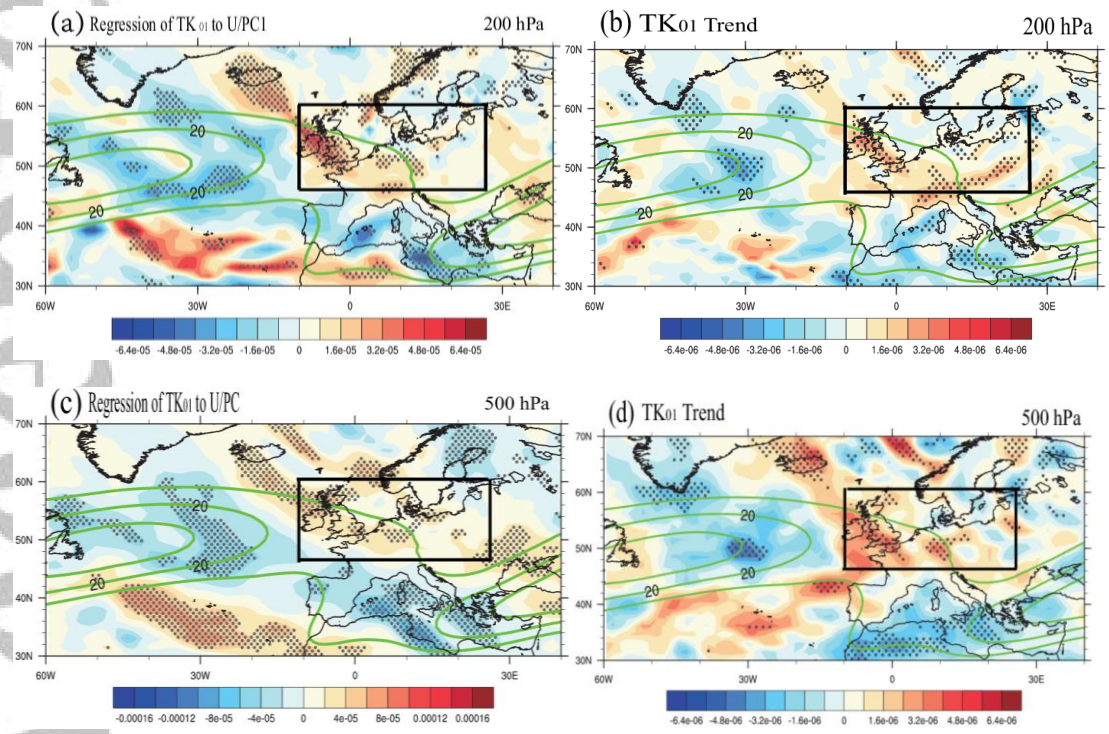

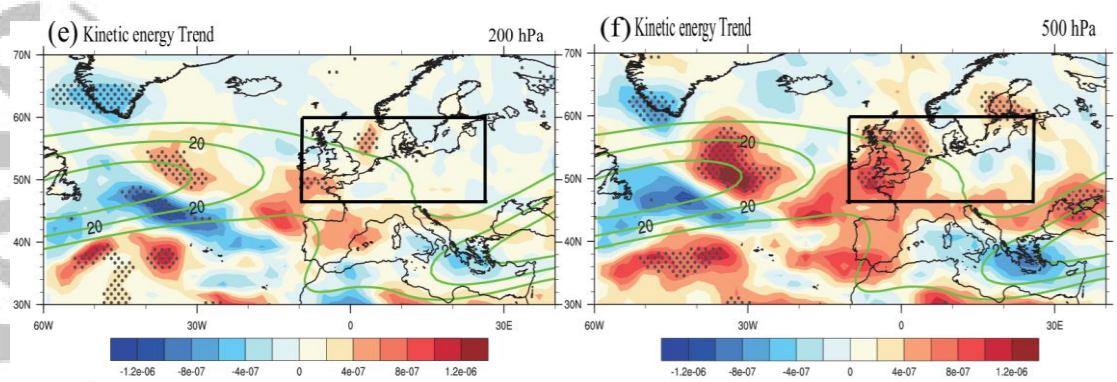

Fig. 5 (a) Regression maps of Tk_{01} at 200 hPa with regard to the U/PC1 (m^2/s^2; shaded). (b) Trend in Tk_{01} at 200 hPa. (c) Same as (a) but at 500 hPa. (d) Same as (b) but at 500 hPa. (e)-(f) Trends of the kinetic energy at 200 hPa and 500 hPa, respectively. The climatological zonal wind, which is greater than 15 m/s, is represented by the green contour. The black dots indicate that the anomalies are significant at the 95% confidence level.

To further verify the relationship between the zonal wind and Tk_{01} from the middle to upper atmosphere, regression maps of Tk_{01} at 200 hPa and 500 hPa with regard to the U/PC1 are shown in Figs. 5(a) and 5(c), respectively. The regressed Tk_{01} at 500 hPa and 200 hPa is positive over the west coast of Europe, including the jet exit, which means that the increasing zonal wind and eastward extension of NAJS favors barotropic kinetic energy convert to seasonal kinetic energy, thus providing adequate kinetic energy for cyclonic eddy growth. In addition, Tk_{01} has an increasing trend in recent decades in the jet exit (Figs. 5(b) and 5(d)), which means that the eastward extension of the NAJS favors barotropic energy conversion from background state to seasonal kinetic energy. In terms of the MS-EVA theory, Tk_{01} is one component of multiscale kinetic energy, is the trend of kinetic energy same as Tk_{01} in the jet exit due to the eastward extension of the NAJS? The trends in the kinetic energy at 500 hPa and 200 hPa are plotted in Figs. 5(e) and 5(f), respectively. Figs. 5(e) and 5(f) show that the kinetic energy has been increasing in recent decades over the jet exit, indicating that the positive trend of the kinetic energy may partly be caused by Tk_{01}. The results

reveal that eastward extension of NAJS favor increasing barotropic energy convert to kinetic energy, which is helpful to cyclonic eddy growth and maintenance of the teleconnection wave train (Williams et al, 2007).

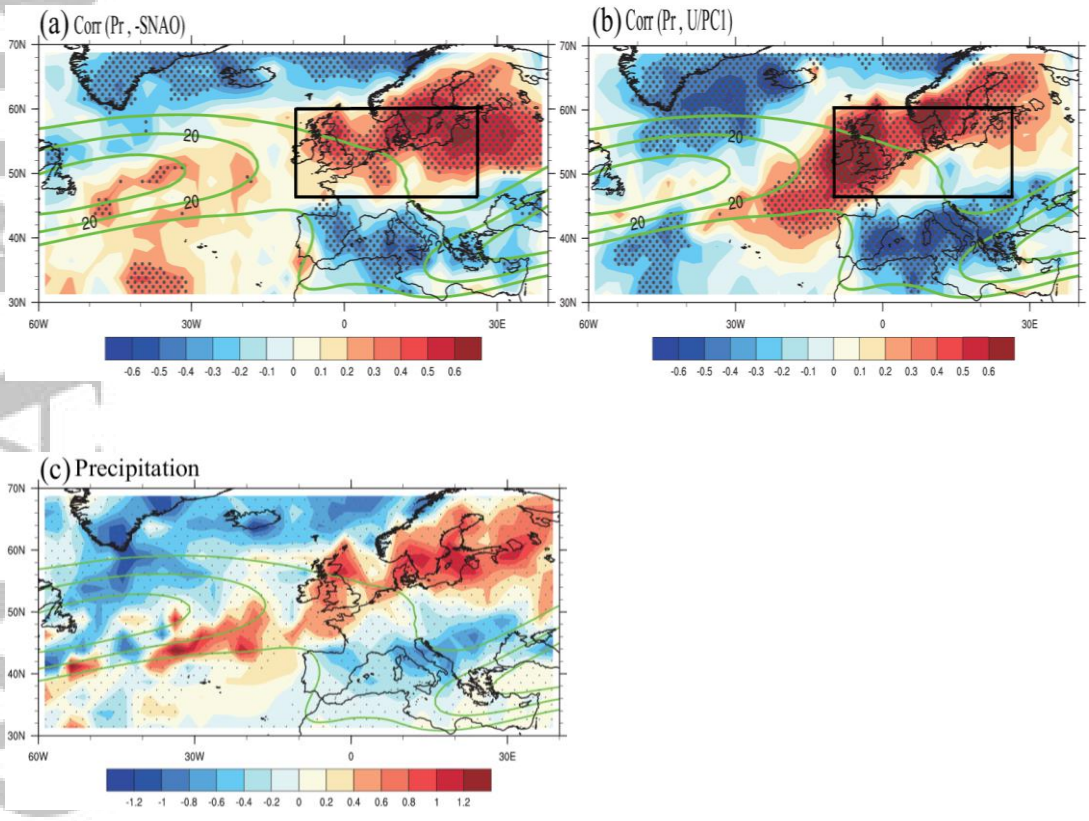

Fig. 6 (a) Correlations between the SNAO index (×-1) and precipitation. (b) Correlations between the U/PC1 and precipitation. (c) Composite differences in precipitation (mm/day; shaded) between the negative-phase SNAO and the mean climate state. The climatological zonal wind, which is greater than 15 m/s, is represented by the green contour. The black dots indicate that the precipitation anomalies are significant at the 95% confidence level.

As described above, anomalous cyclonic circulation at 500 hPa results in the elongation of the trough, which leads to enhanced upward motion and precipitation in the exit. Figures 6(a) and 6(b) show the correlations of the SNAO index (×-1) (multiplications by -1 are used to represent the negative-phase SNAO) with the U/PC1 and precipitation, respectively. The correlation maps show

that there are positive precipitation anomalies over northern Europe, including the jet exit, and negative precipitation anomalies over the Mediterranean region and Greenland when the SNAO is in the negative phase (Fig. 6(a)). This configuration is in agreement with the analysis of Folland et al. (2009) and Blackburn et al. (2008), they proposed the jet steam variability is associated with SNAO and is also implicated in summer European climate. For instance, the summers from 2007 to 2012 produced wet condition over northern Europe, and these associated with a more negative SNAO. In addition to the impact of the SNAO on precipitation, the eastward extension of the NAJS leads to increased precipitation anomalies in the jet exit (Fig. 6(b)). This similar correlation between the NAJS and precipitation has been verified. For example, some studies have found that the southerly North Atlantic storm track is associated with the increasing frequency of floods in northwestern Europe and the increasing frequency of heat waves in the Mediterranean region by affecting the frequency of blocking (Dong et al., 2013; Screen J A., 2013). Figure 6(c) shows composite differences in precipitation between the negative-phase SNAO and the mean climate state. The precipitation anomalies are mainly located near the edge of the jet stream, with increased precipitation (0.6 mm day-1) over the west coast of Europe (40°N-60°N, 0°E-30°E), including the jet exit, and decreased precipitation (0.4 mm day-1) over the Mediterranean area, Greenland, and its surroundings.

Positive precipitation anomalies are beneficial to latent heat release, which favors atmospheric baroclinic instability, particularly in the jet exit. In fact, baroclinic instability could lead to the intensification of atmospheric disturbance activities in the exit, and these disturbance activities could further force the enhancement of upper westerly winds through the internal dynamic process of the atmosphere. Furthermore, the upward motion caused by the enhancement of wind shear can

lead to increased precipitation. This phenomenon seems to be a positive feedback mechanism in the jet exit.

3.3 The mechanisms of the SNAO affecting extreme drought in northern China

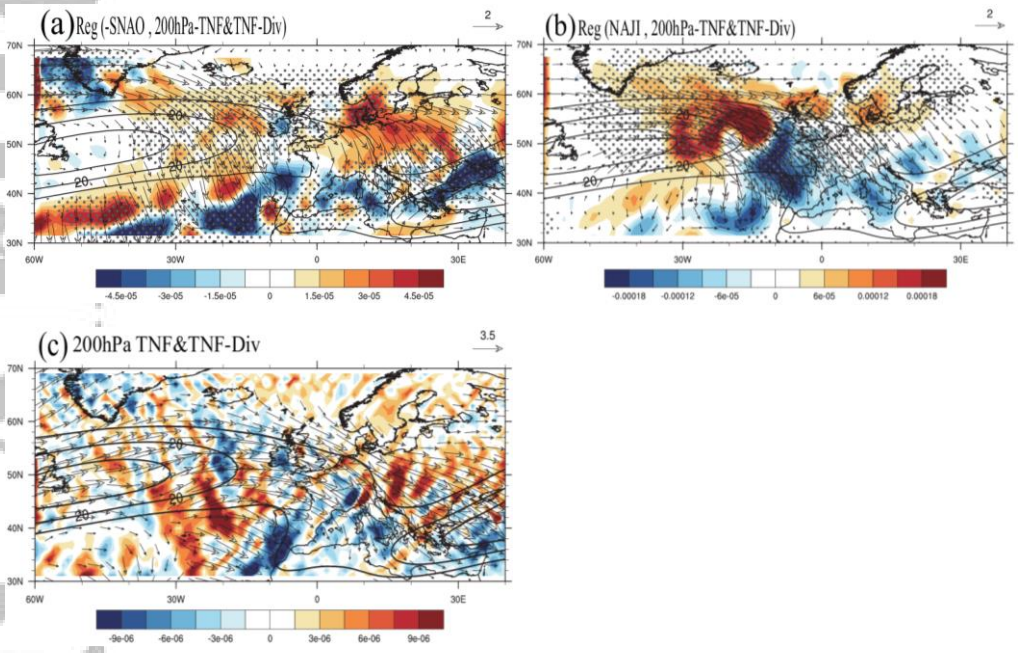

Fig. 7 (a) Regression maps of the TNF (m^2/s^2; vector) and TNF divergence (m/s^2; shaded) at 200 hPa with regard to the NAO index (×-1). (b) Same as (a) but for the NAJS index. (c) Composite anomalies of TNF and TNF divergence in negative SNAO years. The climatological zonal wind, which is greater than 15 m/s, is represented by the black contour. The black dots indicate that the anomalies are significant at the 95% confidence level.

The cyclonic eddy-driven jet enhances the eastward extension of the NAJS, which leads to enhanced zonal wind shear in the jet exit. The NAJS index representing the dynamic effect of cyclonic eddy used in this study is based on the definition by Koch et al. (2006) and Barton (2009) (NAJS positions are averaged over the longitudes 5°E-20°W and latitudes 40°N-50°N in the North Atlantic). To verify the propagation characteristic and the forcing sources of the quasi-stationary wave in the upper troposphere, the regression maps of the TNF and TNF divergence against the

SNAO index (×-1) and NAJS index at 200 hPa are shown in Figs. 7(a) and 7(b), respectively. The horizontal TNF depicts that the wave energy propagated toward the southeast between 40°N and 60°N with a positive divergence TNF centered over the jet exit, which indicates that cyclonic eddy and enhanced wind shear in the jet exit are possible sources of wave energy. In addition, there is also wave energy dispersion in the region with increased precipitation due to the latent heat is released to heat atmosphere and then excite wave energy. The composites of TNF and TNF divergence at 200 hPa in the negative-phase SNAO are displayed in Fig. 7(c). Fig. 7(c) shows that the characteristics of wave energy propagating from the jet exit into the Asian-African jet stream are more obvious, which means that the anomalous Rossby waves excited by the cyclonic eddy may affect northern China through upstream unstable energy fluctuations propagating into the Asian-African jet stream.

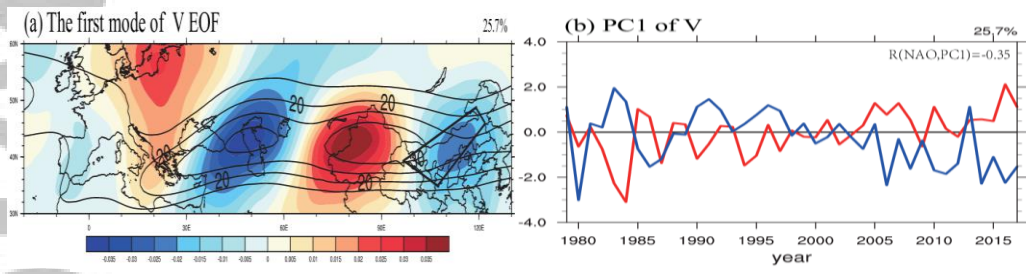

Fig. 8 (a) The leading EOF mode of the 200 hPa meridional wind anomalies in August and (b) normalized leading principal component (PC1). The units are arbitrary. The climatological zonal wind, which is greater than 15 m/s, is represented by the black contour.

The anomalous Rossby waves excited in the jet exit are more likely to enter the Asian-African jet stream, and the SRP zonal teleconnection propagation is restricted to the Asian-African jet stream by the jet waveguide (Lu et al., 2002). What role does the SRP play in the downstream? The spatial distribution of the leading EOF mode in Fig. 8a shows that the centers are located over the Caspian Sea, Mongolia, and northern China, and the latitudes of the three centers are located between 40°N

and 50°N, which is almost consistent with the meridional position of the average Asian-African jet stream. Figure 8(b) indicates that the V/PC1 changes from negative to positive around 2000, which is consistent with previous conclusions (Wang et al. 2017), and has a significant correlation of -0.35 with SNAO at the 95% confidence level. The results reveal that the eastward shift in the negative-phase NAO has a close relationship with wave amplitude.

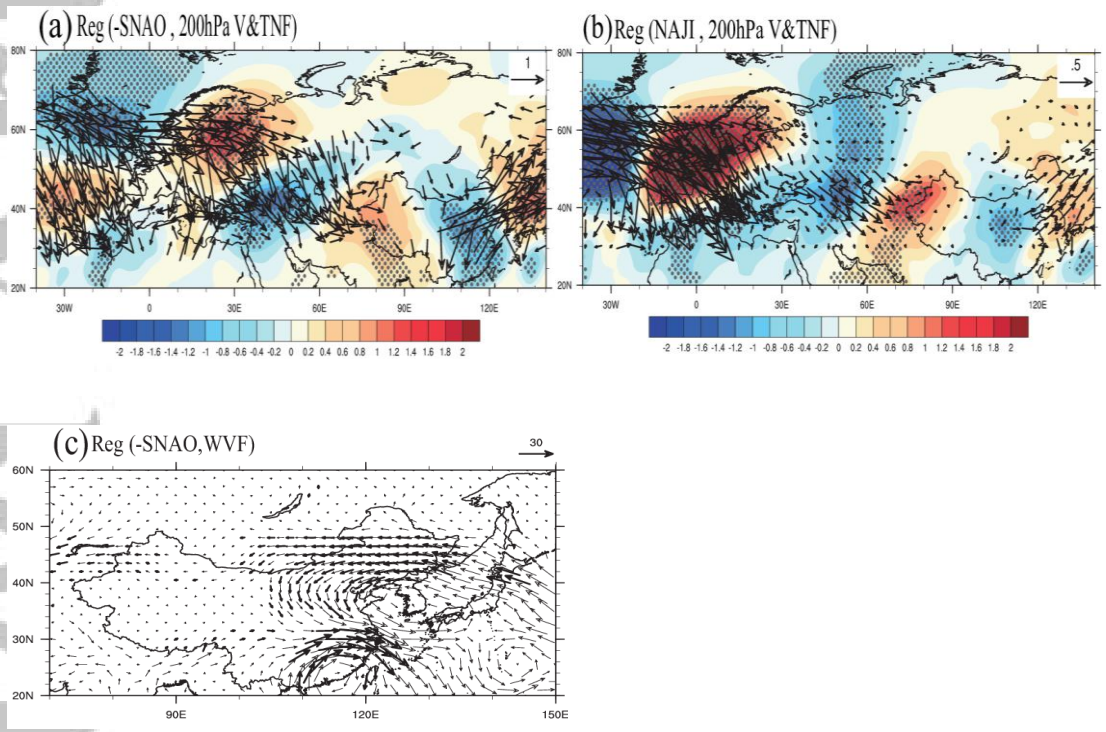

Fig. 9 (a) Regression maps of the 200 hPa meridional wind (m/s; shaded) and TNF (m^2/s^2; vector) with regard to the SNAO (×-1) index. (b) Same as (a) but for the NAJS index. (c) Regression map of the water vapor flux (kg m/s; vector) on the SNAO (×-1) index. The dotted area in (a) and (b) and the black arrows in (c) represent that these regressions are significant at the 95% confidence level.

In general, the anomalous wave energy is more likely to enter the Asian-African jet stream and spread to the downstream region with the SRP. Figure 9 depicts regression maps of the 200 hPa meridional wind and horizontal TNF with regard to the SNAO (×-1) and NAJS index, respectively. According to the regression maps, the negative-phase SNAO and the NAJS could excite the wave

train, similar to SRP corresponding well to magnified wave amplitude and intensity, resulting in favorable eastward propagation of wave energy. The TNF pattern suggests that the SNAO and NAJS-related stationary TNF activities are strong in the jet exit and the anomalous zonal wave energy over the Eurasian continent propagate eastward to northern China. However, wave energy propagating to the east has weakened in central Asia, indicating that there may be other processes involved in this mechanism. From the meridional wind pattern, there are two anomalous anticyclones over the Caspian Sea and northern China and two anomalous cyclones over West Asia and northeastern China. Thus, under the control of anticyclonic circulation over the key region, extreme drought events are more likely to occur. However, a small part of the region (see black box area) is located in northeastern China, where there is anomalous cyclonic circulation. It is possible that the extreme events in this part of the key region could be explained in terms of water vapor transport. Figure 9(c) shows the regression map of the water vapor flux with regard to the SNAO (×-1), suggesting that the water vapor in northern China comes from the northeast, which is unfavorable for water vapor transportation from south to north under the background of mean southwest wind in summer.

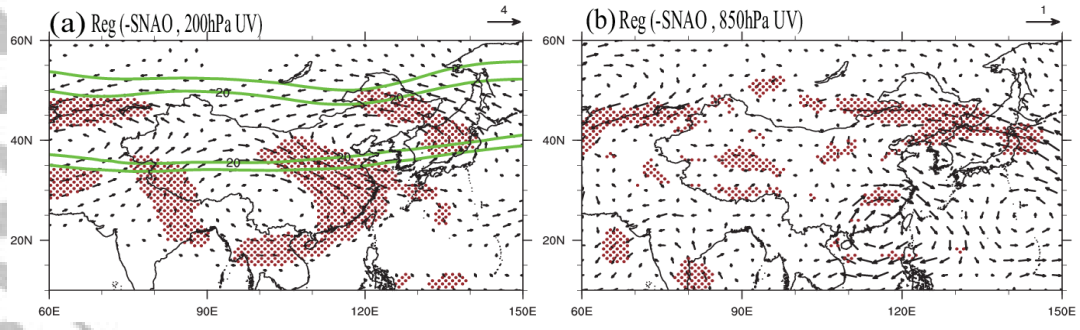

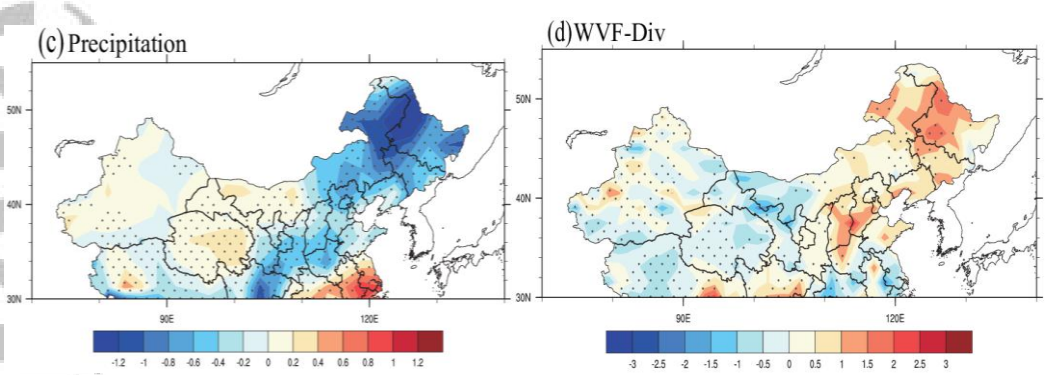

Fig. 10 (a) Regression maps of the zonal and meridional wind anomalies (m/s; vector) at 200 hPa with regard to the SNAO index (×-1). (b) Same as in (a) but for 850 hPa. (c) Composite differences in precipitation (mm/day; shaded) between the negative-phase SNAO and the mean climate state over North China. (d) Same as in (c) but for the vapor flux divergence (kg/(day•m^2•hPa); shaded). The climatological zonal wind, which is greater than 20 m/s, is represented by the green contour in (a). The dots indicate that the winds, precipitation and vapor flux divergence anomalies are significant at the 95% confidence level.

Additionally, the corresponding atmospheric circulation anomalies and climatic impacts in China are shown in Fig. 10. The winds at 200 hPa and 850 hPa are used to characterize the high-level subtropical westerly jet stream and low-level southwest winds of the East Asian summer monsoon (EASM) system, respectively. The structure of the 200 hPa wind field is obvious over eastern-central Asia with an anomalous westerly (easterly) wind near 35°N (50°N) (Fig. 10(a)), which favors an anomalous sinking motion over North China. Meanwhile, anomalous northeasterly winds occur at 850 hPa over North China, which is not beneficial to the transportation of water vapor to the northern area (Fig. 10(b)). It can be concluded from the above results that the atmospheric circulation over North China in the SNAO negative phase is favorable for drought. However, the conditions for extreme drought are more complicated since North China is under the influence of the EASM in summer. Therefore, the vertical precipitation and horizontal

vapor budget are worth considering according to the vapor budget equation. Figures 10(c) and 10(d) show the composite differences in precipitation and vapor flux divergence between the negative-phase SNAO and the mean climate state over North China. The anomalous area of precipitation and water vapor flux divergence is similar in the northern China. The results reveal that the decrease in precipitation and loss of water vapor over the key region further contribute to extreme drought.

3.4 Simulation of the impact of cyclonic circulation anomalies via the LBM

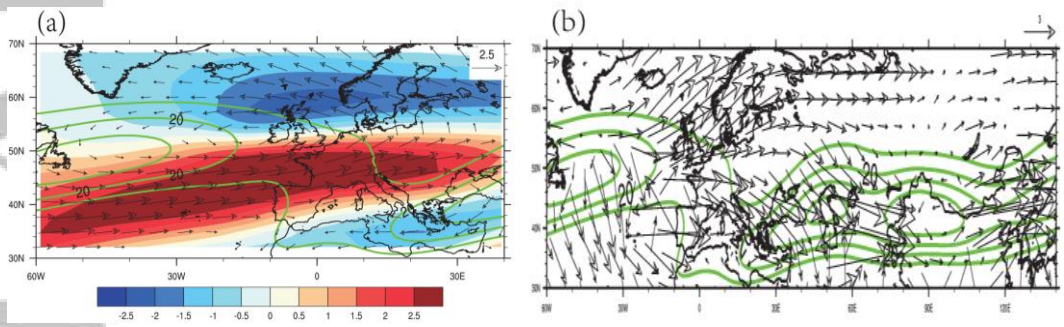

Fig. 11 (a) Responses of the zonal wind (m/s; shaded) and horizontal wind (m/s; vector) at 200 hPa and (b) the TNF (m^2/s^2; vector) to the idealized cyclonic anomalies at 500 hPa over the NAJS exit in a linear baroclinic model. The climatological zonal wind, which is greater than 15 m/s, is represented by the green contour.

Based on the results from the reanalyses and observations, we designed numerical experiments using an LBM forced by cyclonic anomalies at 500 hPa in the jet exit. Fig. 11 displays the responses of the zonal wind, meridional wind, and TNF to the idealized cyclone forcing. The results indicate that the cyclonic eddy-driven jet enhances the eastward extension of the NAJS when the SNAO is in the negative phase. The wind pattern in Fig. 11(a) is similar to that in Fig. 2(c). Fig. 11(b) shows that the wave energy splits into two branches. One of the branches enters the Asian-African jet stream and continues to propagate eastward along with the Asian-African jet stream. The other branch extends from the jet exit to northern Europe and continues to propagate eastward through high

latitudes. The propagation path of the second branch is similar to the Eurasian teleconnection pattern, which can affect the climate of East Asia (Zhang and Chen, 2018).

4. Conclusion

Based on both statistical analyses and model simulations, the intraseasonal relationships among the SNAO and extreme drought over northern China were investigated. Apparently, there exists a significant teleconnection between the eastward shift in the negative-phase SNAO and extreme drought over northern China. Negative SNAO events (SNAO index < -1.0) tend to give rise to extreme drought over northern China, which is related to the anticyclonic anomaly over northern China.

A possible mechanism for this connection between the SNAO and extreme drought events is mainly dependent on cyclonic eddy in the jet exit exciting anomalous Rossby wave energy and spreading into the Caspian Sea, Mongolia, and northern China. Under the background of a negative SNAO, the cyclonic eddy-driven jet enhances the eastward extension of the NAJS in the jet exit at 200 hPa, and the occurrence of barotropic instability results in the transformation of barotropic kinetic energy to seasonal-scale kinetic energy, which provides adequate kinetic energy for cyclonic eddy growth. Meanwhile, the eastward extension of the NAJS leads to enhanced zonal wind shear in the jet exit. In general, upward motion caused by cyclonic circulation at 500 hPa and upper-level wind shear are beneficial to precipitation in the jet exit, which results in the release of latent heat during the period of precipitation, further enhancing the baroclinicity of the atmosphere in the jet exit.

Notably, the Eurasian wave train related to the SNAO is similar to the SRP proposed by Lu (2002). Both wave patterns propagate eastwardly via the subtropical jet stream from the North Atlantic

downstream to the East Asian region. To prove this point, we verified a high correlation between the SNAO and SRP index at the interannual time scale, suggesting that upstream turbulence and remote forcing affect downstream climate anomalies under propagation of stationary wave.

Finally, it is worth noting that we have expressed the characteristics of the interannual time scale in our study. However, some studies have emphasized that the SNAO variations on the interdecadal time scale are also significant (Allen and Folland., 2016; Linderholm and Folland. 2017). Is there a strong correlation between the SNAO and SRP on longer time scales? What are the possible teleconnections among the SNAO and climate anomalies over northern China on longer time scales? These questions need to be explored in future studies.

Acknowledgments

This research was jointly supported by the National Key R&D Program of China (Grant No. 2018YFC1507101), the National Natural Science Foundation of China (Grant No. 41975083) and the Key Program (Grant No. 41630426). The ERA-Interim data set is available online (http://apps.ecmwf.int/datasets). The monthly mean NAO indices are acquired from website (ftp://ftp.cpc.ncep.noaa.gov/cwlinks).The sc-PDSI data is available on line (https://climatedataguide.ucar.edu/climate-data/palmer-drought-severity-index-pdsi).

References

Allan, R. and C, K, Folland. (2016). Atmospheric circulation. 1. Sea level pressure [in "State of the Climate 2015"]. Bull. Amer. Meteor. Soc., 97, S36–S38.

Barton, N. P. & Ellis, A. W. (2009). Variability in wintertime position and strength of the North Pacific jet stream as represented by re-analysis data. International Journal of Climatology, 29, 851–862.

Blackburn, M., Methven, J., Roberts, N. (2008). Large-scale context for the UK floods in summer 2007. Weather, 63(9), 280–288.

Byun, H, and R., D, A, Wilhite. (1999). Objective quantification of drought severity and duration. Journal of Climate, 12, 2747-2756, doi:10.1175/1520-0442012, 2747: OQODSA.2.0.CO;2.

Chen, G., R, Huang. (2012). Excitation mechanisms of the teleconnection patterns affecting the July precipitation in northwest China. Journal of Climate, 25, 7834-7851, doi:10.1175/ JCLI-D-11-00684.1.

Dai. (2011b). Characteristics and trends in various forms of the Palmer drought severity index during 1900–2008. Journal of Geophysical Research, 116, D12115, doi:10.1029/2010JD015541.

Dai. K, E, Trenberth., T, R, Karl. (1998). Global variations in droughts and wet spells: 1900-1995. Geophysical Research Letters, 25, 3367-3370, doi:10.1029/98GL52511.

Dong, B. W., Sutton, R. T., Woollings, T. & Hodges, K. (2013). Variability of the North Atlantic summer storm track: mechanisms and impacts on European climate. Environmental Research Letters, 8, 034037.

Eastin, M, D., Vincent, D, G. (1998). A 6-Yr Climatology of Vertical Mean and Shear Components of Kinetic Energy for the Australian–South Pacific Jet Stream. Journal of Climate, 11(2), 283-291.

Edwards, D, C., T, B, McKee., (1997). Characteristics of 20th century drought in the United States at multiple time scales. Department of Atmospheric Science, Colorado State University, Atmospheric Science Paper 634, 155 pp.

Folland, C, K., Knight, J., Linderholm, H, W., Fereday, D., Ineson, S., Hurrell, J, W. (2009). The Summer North Atlantic Oscillation: past, present and future. Journal of Climate, 22, 1082–1103.

Gu, W., Li, C., Li, W., Zhou, W., Chan, L. (2009). Interdecadal unstationary relationship between NAO and east China's summer precipitation patterns. Geophysical Research Letters, 36, L13702, doi:10.1029/2009GL038843.

Hall, R., Erdelyi, R., Hanna, E., Jones, J, M., Scaife, A, A. (2014). Drivers of North Atlantic Polar Front jet stream variability. International Journal of Climatology, 35(8), 1697-1720.

He, B., A, F, Lü., J, Wu., L, Zhao., M, Liu. (2011). Drought hazard assessment and spatial characteristics analysis in China. Journal of Geographical Sciences, 21, 235-249, doi:10.1007/s11442-011-0841-x.

Hong, X., Lu, R., Li, S, L. (2017). Amplified summer warming in Europe–West Asia and Northeast Asia after the mid-1990s. Environmental Research Letters, 12, 094007.

Hsu, P, C., Tsou, C, H., Hsu, H, H. (2009). Eddy Energy along the Tropical Storm Track in Association with ENSO. Journal of the Meteorological Society of Japan, 87(4), 687-704.

Huang, R., Chen, J., Huang, G. (2007). Characteristics and variations of the East Asian monsoon system and its impacts on climate disasters in China. Advances in Atmospheric Sciences, 24, 993–1023.

Hurrell, J, W. (1995). Decadal trends in the North Atlantic Oscillation: Regional temperatures and precipitation. Science, 269, 676–679.

Hurrell, J, W., H, Van, Loon. (1997). Decadal variations in climate associated with the North Atlantic Oscillation. Climatic Change, 36, 301–326.

Hurrell, J, W., Folland, C, K. (2002). A change in the summer atmospheric circulation over the North Atlantic. Clivar Exchanges, 25, 1–3.

Koch, P., Wernli, H. & Davies, H, C. (2006). An event-based jet-stream climatology and typology. International Journal of Climatology, 26, 283–301.

Lau, K, H., and Lau, N, C. (1992). The Energetics and Propagation Dynamics of Tropical Summertime Synoptic-Scale Disturbances. Monthly Weather Review, 120(11), 2523.

Lee, S, M., H, R, Byun., H, L, Tanaka. (2012). Spatiotemporal characteristics of drought occurrences over Japan. Journal of Applied Meteorology and Climatology, 51, 1087-1098, doi:10.1175/JAMC-D-11-0157.1.

Linderholm, H, W., T, Ou., J-H, Jeong., C, K, Folland., et al. (2011). Interannual teleconnections between the summer North Atlantic Oscillation and the East Asian summer monsoon. Journal of Geophysical Research, 116, D13107, doi:10.1029/2010JD015235.

Li, J., Sun, C., Jin F. (2013). NAO implicated as a predictor of Northern Hemisphere mean temperature multidecadal variability. Geophysical Research Letters, 40, 5497–5502, doi:10.1002/2013GL057877.

Liang, X., and A, R, Robinson. (2005). Localized multiscale energy and vorticity analysis. Dynamics of Atmospheres and Oceans, 38, 195–230, doi:10.1016/j.dynatmoce.2004.12.004.

Liang X. (2016). Canonical transfer and multiscale energetics for primitive and quasi-geostrophic atmospheres. Journal of Atmospheric Sciences, 73(11), 4439-4468.

Liang, X., and A, R, Robinson. (2007). Localized multi-scale energy and vorticity analysis: II. Finite-amplitude instability theory and validation. Dynamics of Atmospheres and Oceans, 44, 51–76, doi:10.1016/j.dynatmoce.2007.04.001.

Linderholm, H., and C, K, Folland. (2017). Summer North Atlantic Oscillation (SNAO) variability on decadal to palaeoclimate time scales. Past Global Changes Mag, 25, 57-60, https:// doi.org/10.22498/pages.25.1.57.

Lu, R., OH, J, H., Kim, B, J. (2002). A teleconnection pattern in upper-level meridional wind over the North African and Eurasian continent in summer. Tellus A: Dynamic Meteorology and Oceanography, 54(1), 44-55.

Ma, Z., Fu, C. (2006). Some evidence of drying trend over northern China from 1951 to 2004. Chinese Science Bulletin, 51, 2913–2925.

McKee, T, B., N, J, Doesken., and J, Kleist., (1993). The relationship of drought frequency and duration to time scales. Proc.8th Conference. on Applied Climatology, 179–184.

Nitta, T. (1987). Convective activities in the tropical western Pacific and their impact on the NH summer circulation. Journal of the Meteorological Society of Japan, 65, 373–390.

Oh, S, B., H, R, Byun., and D, W, Kim. (2014). Spatiotemporal characteristics of regional drought occurrence in East Asia. Theoretical and applied climatology, 117, 89-101, doi:10.1007/s00704-013-0980-3.

Palmer, W, C. (1965). Meteorologic drought. U.S. Department of Commerce, Weather Bureau, Research Paper 45, 58 pp.

Panagiotis, Angelidis., Fotios, Maris., Nikos, Kotsovinos., et al .(2012). Computation of Drought Index SPI with Alternative Distribution Functions. Water Resources Management, 26, 2453–2473.

Qiao, S., Feng, G. (2016). Impact of the December North Atlantic Oscillation on the following February East Asian trough. Journal of Geophysical Research, 121, 10074–10088, https://doi.org/10.1002/2016J D025007.

Rogers, J, C. (1997). North Atlantic storm track variability and its association to the North Atlantic Oscillation and climate variability of northern Europe, Journal of Climate, 10(7), 1635–1647.

Sasaki, Y, N., Minobe, S., Schneider, N. (2012). Decadal Response of the Kurishio Extension Jet to Rossby Waves: Observation and Thin-jet Theory. Journal of Physical Oceanography, 43(2),442-456.

Screen J A. (2013). Influence of Arctic sea ice on European summer precipitation. Environmental

Research Letters, 8,044015.
Sun, J. Q., Wang H., Yuan, W. (2008a). Decadal variations of the relationship between the summer North Atlantic Oscillation and middle East Asian air temperature. Journal of Geophysical Research, 113, D15107, doi:10.1029/2007JD009626.
Sun, J. Q., and Wang, H. (2012). Changes of the connection between the summer North Atlantic Oscillation and the East Asian summer rainfall. Journal of Geophysical Research, 117, D08110, doi:10.1029/2012JD017482.
Sun, J. Q., Wang H., and Yuan W. (2009b). A possible mechanism for the co-variability of the boreal spring Antarctic Oscillation and the Yangtze River valley summer rainfall. International Journal of Climatology, 29(9), 1276–1284, doi:10.1002/joc.1773.
Takaya, K., and H, Nakamura. (1997). A formulation of a wave-activity flux for stationary Rossby waves on a zonally varying basic flow. Geophysical Research Letters. 24, 2985-2988, doi:10.1029/97GL03094.
Takaya, K., and H, Nakamura. (2001). A formulation of a phase-independent wave activity flux for stationary and migratory quasigeostrophic eddies on a zonally varying basic flow. Journal of Atmospheric Sciences, 58, 608–627.
Trenberth et al. (2014). Global warming and changes in drought. Nature Climate Change, 4, 17-22.
Thom (1958). A Note on the Gamma Distribution. Monthly Weather Review, pp 117-122.
Wang, C., Yang, K., Li, Y., Wu, D., & Bo, Y. (2017). Impacts of spatiotemporal anomalies of Tibetan Plateau snow cover on summer precipitation in eastern China. Journal of Climate, 30(3), 885–903. https://doi.org/10.1175/JCLI-D-16-0041.1
Walker, G, T. (1924) Correlation of seasonal variations in weather IX: a further study of world weather. Mem Indian Meteor Dep 24, 275-332.
Wang, Z, Q., Yang, S. Lau, N, C., Duan, A, M. (2018). Teleconnection between summer NAO and East China rainfall variations: a bridge effect of the Tibetan Plateau. Journal of Climate, 31(16), 6433–6444.
Wallace, J, M., and D, S, Gutzler. (1981). Teleconnections in the geopotential height field during the Northern Hemisphere winter. Monthly Weather Review, 109(4), 784-812.
Wang, L., Xu, P., Chen, W., et al. (2017). Interdecadal Variations of the Silk Road Pattern. Journal of Climate, 30(24), 9915-9932.
Wei,F,Y. (2007). Modern climate statistical diagnosis and prediction technology (Second Edition, in chinese). China Meteorological Press.
Williams, R, G., Wilson, C., Hughes, C, W. (2007). Ocean and Atmosphere Strom Tracks:The Role of Eddy Vorticity Forcing. Journal of Physical Oceanography, 37(9), 2267-2289.
Wiin-Nielsen, A. and Drake, M. (1965). On the energy exchange between the baroclinic and barotropic components of atmospheric flow. Monthly Weather Review, 9(2), 79-92.
Woollings, T., and M, Blackburn. (2012). The North Atlantic jet stream under climate change and its relation to the NAO and EA patterns. Journal of Climate, 25, 886-902.
Wu, B., Wang, J. (2002). Winter Arctic Oscillation, Siberian High and East Asian winter monsoon. Geophysical Research Letters, 29, 1897, https://doi.org/10.1029/2002G L015373.
Wu, B., Zhou, T., Li, T. (2009). Seasonally evolving dominant interannual variability modes of East Asian climate. Journal of Climate, 22, 2992-3005.
Wu, Z., Wang, B., Li, J., Jin, F. (2009). An empirical seasonal prediction model of the East Asian

summer monsoon using ENSO and NAO. Journal of Geophysical Research, 114, D18120, https://doi.org/10.1029/2009J D011733.

Xu, P., Wang, L., Chen, W. (2019). The British-Baikal Corridor: a teleconnection pattern along the summertime polar front jet over Eurasia. Journal of Climate, 32(3), 877-896.

Yuan, W., and J, Q, Sun. (2009). Enhancement of the summer North Atlantic Oscillation influence on Northern Hemisphere air temperature. Advances in Atmospheric Sciences, 26(6), 1209-1214, doi:10.1007/s00376-009-8148-x.

Zhai, J., B, Su., V, Krysanova., T, Vetter, C, Gao., T, Jiang., (2010). Spatial variation and trends in PDSI and SPI indices and their relation to streamflow in 10 large regions of China. Journal of Climate, 23, 649-663, doi:10.1175/2009JCLI2968.1.

Zhang, C., B, Wang. D, Liu., Z, Cai. (1998). Research on drought and flood indices in the northwest China (in Chinese). Plateau Meteorology, 17, 381-389.

Zhang, J., H, Chen., S, Zhao. (2019). A tripole pattern of summertime rainfall and the teleconnections linking northern China to the Indian subcontinent. Journal of Climate, 32, 3637-3653, DOI:10.1175/JCLI-D-18-0659.

Zhang, J., H, Chen., Q, Zhang. (2018). Extreme drought in the recent two decades in northern China resulting from Eurasian warming. Climate Dynamics, 52, 2885-2902, DOI: 10.1007/s00382-018-4312-2.

Zhang, J., Li, L., Li, D., Deng, W. (2015). Summer droughts in the north portion of the Yellow river basin in association with recent Arctic ice loss. International Journal of Climatology, 35, 2849-2859.

Zhang, L., and Zhou, T. (2015). Drought over East Asia: a review. Journal of Climate, 28(8), 3375-3399.

Zhang, Q., X, Zou., F, Xiao. (2006). Classification of meteorological droughts. Standards Press of China Tech, Rep, GB/T20481-2006, 17pp.

Zhang, Q., Coauthors. (2009). Drought (in Chinese). China Meteorological Press, 199 pp.

Zuo, J., Ren, H., Li, W. (2015). Contrasting impacts of the Arctic Oscillation on surface air temperature anomalies in southern China between early and middle-to-late winter. Journal of Climate, 28, 4015-4026.

Zuo, J., Ren, H., Li, W., Wang, L. (2016). Interdecadal Variations in the relationship between the Winter North Atlantic Oscillation and Temperature in South-Central China. Journal of Climate, 29, 7477-7493.

Zuo, J., Li, W., Sun, C., Xu, L., Ren, H. (2013). Impact of the North Atlantic sea surface temperature tripole on the East Asian summer monsoon. Advances in Atmospheric Sciences, 30, 1173-1186.

Zou, X., Q, Zhang. (2008). Preliminary studies on variations in droughts over China during past 50years (in Chinese). Journal of applied meteorology and climatology, 19, 679-687.